



Actuators and Sensors Based on Tensegrity D-bar Structures

Utku Boz¹, Raman Goyal² and Robert E. Skelton^{2*}

¹ Department of Mechanical Engineering, University of Wisconsin at Madison, Madison, WI, United States, ² Department of Aerospace Engineering, Texas A&M University, College Station, TX, United States

OPEN ACCESS

Edited by:

Behcet Acikmese,
University of Washington,
United States

Reviewed by:

Shu Yang,
Northwestern Polytechnical University,
China
Makoto Ohsaki,
Kyoto University, Japan
Xiaotian Shi,
University of Washington,
United States

*Correspondence:

Robert E. Skelton
bobskelton@tamu.edu

Specialty section:

This article was submitted to
Space Robotics,
a section of the journal
Frontiers in Astronomy and Space
Sciences

Received: 08 May 2018

Accepted: 26 November 2018

Published: 13 December 2018

Citation:

Boz U, Goyal R and Skelton RE (2018)
Actuators and Sensors Based on
Tensegrity D-bar Structures.
Front. Astron. Space Sci. 5:41.
doi: 10.3389/fspas.2018.00041

Tensegrity offers lightweight deployable structures for use in many engineering disciplines. Among all of the available tensegrity forms, *D-Bar* has a potential for combined applications of sensing, actuation, and structural support. In this paper, we enhance the minimal mass formulation of the *D-Bar* by including yielding of the compressive members as a design constraint in contrast to the previous assumption which considers buckling as the sole failure mechanism. In addition, we analyze the length and force gains of a *D-bar* system analytically by considering the minimal mass *D-bar* as the design constraint. Furthermore, we calculate the stiffness of the *D-Bar* and when appropriate use as design constraints as well. To enhance the minimal mass properties of the *D-Bar*, we combine T-bar and D-bar systems. The analysis shows that these structures are the basis for effective force transducers, force-controlled actuators, and efficient deployable compressive structures.

Keywords: tensegrity, D-bar systems, stiffness, actuators, sensors

1. INTRODUCTION

We consider tensegrity as any network of axially-loaded prestressable members (Skelton and de Oliveira, 2009). Tensegrity structures are proven to be minimum mass for various loading conditions (Skelton and de Oliveira, 2009). It is important to minimize the mass of structure for space applications. Therefore, tensegrity can be used to provide solutions to many structural problems in space, such as artificial gravity space habitats (Skelton and Longman, 2014; Goyal et al., 2017), minimum mass structures for space (Skelton and de Oliveira, 2010; Nagase and Skelton, 2014), and impact lander for planetary explorations (SunSpiral et al., 2013; Rimoli, 2016).

Tensegrity structures offer various functions such as load-bearing, sensing, actuation, and morphing capabilities (Skelton and de Oliveira, 2009). Moreover, by selecting different material for each member of the network or using various combinations of materials, it is possible to create structures with special electrical, acoustic or mechanical properties. Early tensegrity contributors include (Snelson, 1965; Fuller et al., 1975; Pugh, 1976; Calladine, 1978; Pellegrino, 1986; Murakami and Nishimura, 2001; Sultan and Skelton, 2004; Motro, 2011). Efficient models for tensegrity dynamics are proposed in Skelton (2005) and Goyal and Skelton (2018) representing the dynamics of tensegrity structures with a new matrix form and shape-changing control strategies.

Beyond minimal mass properties, there are studies showing the suitability of tensegrity structures for sensing and actuation. Sultan and Skelton used an icosahedron tensegrity structure to develop a 6 d.o.f sensor structure (Sultan and Skelton, 2004). They employed tendons of the tensegrity structure as sensing members and showed that the tensegrity structure is capable of measuring the forces and torques in all directions. Furthermore, they proved that a tensegrity structure offers fault-tolerant, redundant architecture for more precise measurement of the

environmental loading conditions. Hagiwara and Oda (2010) used the tendons of the tensegrity prism as actuators to transform a structure between different configurations. They numerically and experimentally evaluated the capabilities of a tensegrity prism for form-finding applications and showed its promising structural concept for robotic applications. A recent study by Koizumi et al. (2012) demonstrates a tensegrity robot that is driven by soft actuators. They employed pneumatic actuators to experimentally demonstrate the capability of the tensegrity mechanism to perform the requested motion path on a flat surface.

The D-bar tensegrity topology introduced in Skelton and de Oliveira (2009) is investigated here further for its use in sensing and actuating functions. First, the minimal mass design for the D-Bar is extended to include the yielding as a possible failure mechanism as the number of complexity is increased. Then, using the minimal mass configuration, an analytical framework is developed to utilize the D-Bar as a sensor or actuator for either length or force under compressive configuration using structural parameter relations. Later, as an essential element to any sensor or actuator, formulation to evaluate the stiffness of the structure is derived for compressive performance. Finally, a novel structure configuration combining T-Bar and D-Bar is proposed and a brief overview of its minimal mass properties and parametric relations as well as its stiffness properties are presented. For each step of derivation, detailed examples are provided to illustrate the potential use of the proposed structural paradigm based on tensegrity D-Bar.

The paper is organized as follows. Section 2 describes the D-Bar, the concept of self-similarity, and reviews the minimal mass properties of the tensegrity D-Bar under buckling constraints. sections 3 derives the analytical relations between structural parameters of D-bar as sensors and actuators for planar and 3D D-Bar networks. Section 4 presents the stiffness formulation for the planar and 3D D-Bar and section 5 determines the minimum mass to satisfy a given stiffness requirement in the planar configuration. Section 6 describes the novel configuration combining the planar T-Bar and D-Bar. Section 7 gives an example to design minimal mass loaded platform to deploy to a specified shape. Finally, section 8 provides some conclusions.

2. MINIMAL MASS D-BAR UNDER COMPRESSIVE LOADING FOR BUCKLING CONSTRAINTS

Figure 1 illustrates a D-bar structure of complexity 1. There are 4 compressive members (bars) and 1 tensile member (string) in the structure, where L is the length of the D-Bar, l_b is the bar length and s is the string length. It has been shown Skelton and de Oliveira (2009) that, for complexity $q = 1$, and any given applied force F , the normalized mass ratio (μ) under buckling constraints is given by:

$$\mu = (2 \cos^5 \alpha)^{-1/2} + \epsilon (\tan^2 \alpha), \tag{1}$$

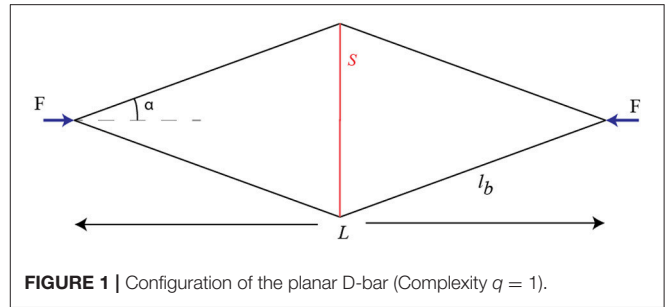


FIGURE 1 | Configuration of the planar D-bar (Complexity $q = 1$).

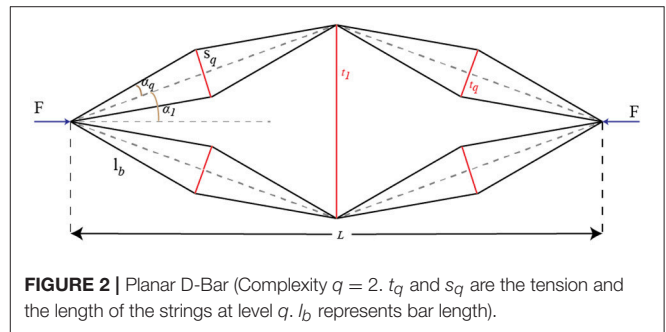


FIGURE 2 | Planar D-Bar (Complexity $q = 2$). t_q and s_q are the tension and the length of the strings at level q . l_b represents bar length).

where μ is the ratio of the mass of the D-bar system and the minimal mass of a solid bar that could take the same external load. The term ϵ includes the material properties, the magnitude of the compressive force, and overall length of the structure and is defined as:

$$\epsilon = \frac{\sqrt{\pi} \rho_s \sqrt{E_b} \sqrt{F}}{2 \sigma_s \rho_b L}, \tag{2}$$

where ρ_s and ρ_b are mass densities of the string and bar materials, respectively. E_b is the elastic modulus of the bar material, σ_s is the yield stress of the string material and L is the length of the D-Bar. When $\mu < 1$, the D-bar system has less mass than a single bar that could take the same load. The necessary condition for mass ratio to be less than 1 is $\sqrt{2} \cos^{\frac{5}{2}} \alpha > 1$ or equivalently $\alpha < 29.477^\circ$. Therefore, for $\mu < 1$, one can replace any bar in a structure with this D-bar, where, each bar is replaced with yet another D-bar. This procedure is called *self-similar iteration*. A structure obtained after q self-similar iterations is called a *D-bar system of complexity q* .

Figure 2 shows a D-bar system of complexity $q = 2$, where a different α is used for 2nd iteration. The strings of the D-Bar fail due to yielding, but the bars may fail due to either yielding or buckling. For a complexity q planar D-bar, with different choices for α at each self-similar iteration, the normalized mass at the buckling constraint is given in Skelton and de Oliveira (2009) as:

$$\mu = 2^{2q} \left(\frac{1}{\prod_{i=1}^q (2 \cos \alpha_i)} \right)^{5/2} + \epsilon \sum_{i=1}^q \frac{2^{2i-2} \tan^2 \alpha_i}{[\prod_{j=1}^{i-1} (2 \cos \alpha_j)]^2}. \tag{3}$$

Figure 3 shows a special case of the D-Bar structures where angles are equal on each complexity level ($\forall \alpha_i = \alpha$). Note that

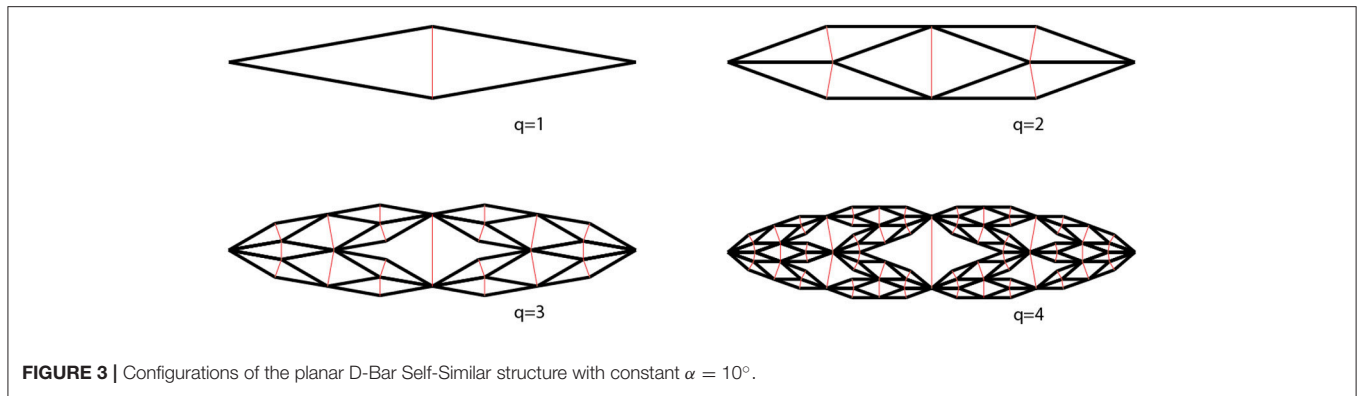


FIGURE 3 | Configurations of the planar D-Bar Self-Similar structure with constant $\alpha = 10^\circ$.

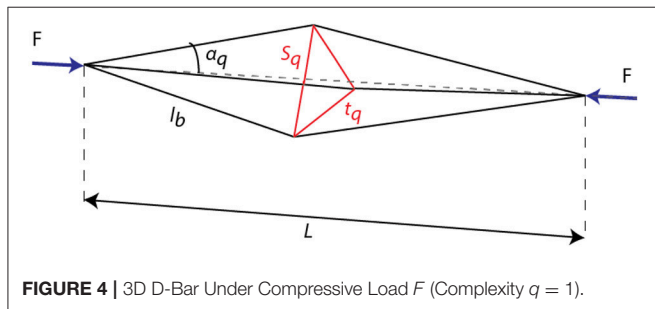


FIGURE 4 | 3D D-Bar Under Compressive Load F (Complexity $q = 1$).

TABLE 1 | Material properties.

	Aluminum	UHMWPE
ρ ($\frac{kg}{m^3}$)	2,700	970
E ($\frac{N}{m^2}$)	60×10^9	120×10^9
σ_{yield} ($\frac{N}{m^2}$)	110×10^6	2.7×10^9

to ensure the same angle for each self-similar iteration during the application, the duplicate members can be combined into a single member.

When the same angle α is used for self-similarity, the normalized mass from Equation (3) for any complexity q reduces to:

$$\mu = (2 \cos^5 \alpha)^{-q/2} + \epsilon(\cos^{-2q} \alpha - 1). \tag{4}$$

For the three dimensional (3D) D-Bar shown in Figure 4, for the special case $\forall \alpha_i = \alpha$, Equation (4) is modified as follows:

$$\mu_{3D}^N = \left(\frac{4 \cos^5 \alpha}{N} \right)^{-q/2} + \epsilon(\cos^{-2q} \alpha - 1), \tag{5}$$

where subscript is used to represent the 3D configuration. The term N appearing in Equation (5) stands for maximum number of bars connected to the same point when $q = 1$. For example, $N = 3$ for the D-Bar configuration shown in Figure 4.

As previously stated, the mode of failure in the bars can be yielding or buckling depending on the configuration or the force applied. For any D-Bar system of complexity q , yielding becomes the mode of failure if the following inequality is satisfied as shown in the Skelton and de Oliveira (2009):

$$\frac{F}{L^2} > \frac{4\sigma_b^2}{\pi E_b(2 \cos \alpha)^q}. \tag{6}$$

For the 3D D-Bar, following the same procedure for the derivation of Equation (6) as described in Skelton and de Oliveira

(2009) the same condition changes to:

$$\frac{F}{L^2} > \frac{4\sigma_b^2}{\pi E_b(\frac{4}{N} \cos \alpha)^q}. \tag{7}$$

Clearly, these equations show that yielding becomes the mode of failure if complexity q is large enough.

Example 1: Consider the material properties given in Table 1 for bars and strings (Aluminum for bars and Ultra High Molecular Weight Polyethylene (UHMWPE) for strings). Figures 5A,B show the limit values of $\frac{F}{L^2}$ for planar and 3D D-Bars, respectively, by considering 3 different angular configurations $\alpha = 10^\circ, 15^\circ$ and 20° . The shaded region indicates the area satisfying the inequalities (6) and (7). The primary mode of failure changes from buckling to yielding when the $\frac{F}{L^2}$ is greater than value of the line specific to each angular configuration.

Planar D-Bar changes its primary mode of failure for lower values of $\frac{F}{L^2}$ than the 3D D-Bar. On the other hand, the higher the angle, the higher the value of $\frac{F}{L^2}$ before the mode of failure changes from buckling to yielding.

3. STRUCTURAL PARAMETER RELATIONS OF D-BAR AS SENSOR AND ACTUATOR

This section provides the relationship between the structural parameters of the D-Bar. For the remainder of the paper, it is assumed that bars are rigid, strings are elastic, and the mass of the joints is negligible. Figures 2, 4 shows the general form of the D-bar under compressive loading.

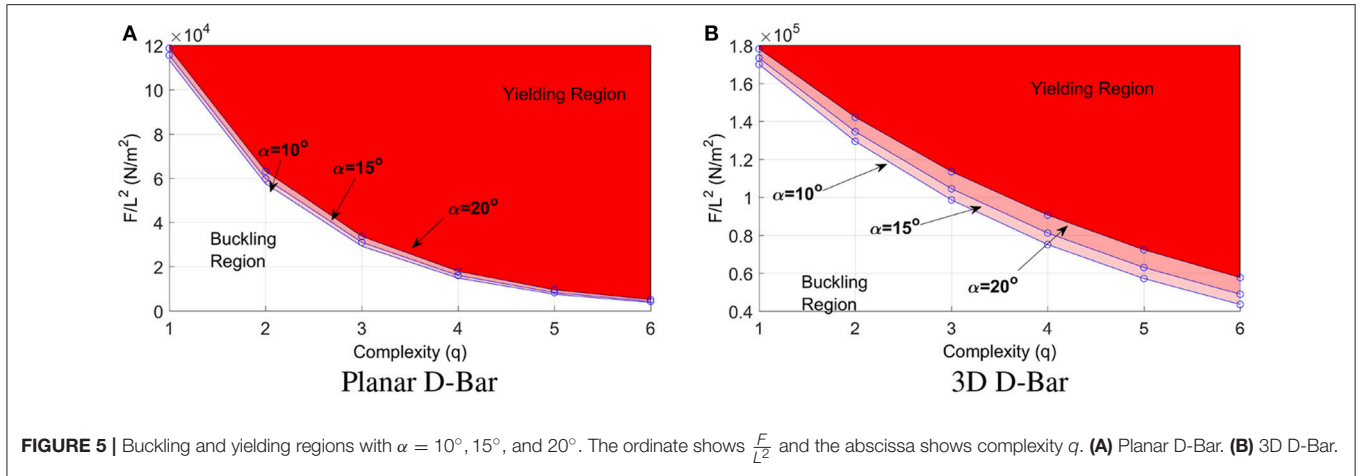


FIGURE 5 | Buckling and yielding regions with $\alpha = 10^\circ, 15^\circ,$ and 20° . The ordinate shows $\frac{F}{L^2}$ and the abscissa shows complexity q . **(A)** Planar D-Bar. **(B)** 3D D-Bar.

3.1. Length Gain : $\Delta L / \Delta S_q$

The length of the D-Bar is specified by the configuration of its structural members. Given that the overall length L of the D-Bar changes with the compression, it is possible to quantify the overall length change by tracking the length change over the strings of the D-Bar. The strings of the D-Bar undergo the same length change in the same complexity level. Since there are more than one strings when the complexity level is bigger than 1, it is possible to measure the same quantity using multiple structural members. This property of the D-Bar makes it suitable displacement sensor with many equivalent outputs. Therefore, the sensor configuration is robust because it is possible to measure the displacement even when one or more sensor structural members fail. Furthermore, the versatility of the D-Bar ensures the actuation performance governed by exactly the same relations for displacement.

Theorem 1: The Gain $G_1(q)$, defined as the ratio of change in length of the D-bar to change in length of the shortest string at complexity q , is given by:

$$G_1(q) = \frac{\Delta L}{\Delta S_q} = \frac{\Xi - \Xi_0}{2(\sin(\alpha_q) - \sin(\alpha_{q0}))}, \quad (8)$$

where $\Xi = \prod_{i=1}^q 2 \cos(\alpha_i)$, $\Xi_0 = \prod_{i=1}^q 2 \cos(\alpha_{i0})$, α_{i0} is the initial angle at complexity level i and α_i is the final angle at complexity level i after the D-Bar is statically balanced. The extension of the same relation to the 3D D-Bar, G_1^{3D} is given as:

$$G_1^{3D}(q) = \frac{\Delta L^{3D}}{\Delta S_q^{3D}} = \frac{\Xi^{3D} - \Xi_0^{3D}}{2(\sin(\alpha_q^{3D}) - \sin(\alpha_{q0}^{3D}))(\cos(\frac{N\pi - 2\pi}{2N}))}, \quad (9)$$

where the superscript 3D indicates that the relations are derived for the three dimensional case.

Proof: Recalling the rigid bar assumption, we can formulate the geometrical relations between the bar length l_b , initial length of the D-bar L_0 , final length of the D-bar L and angles α_i, α_{i0} as:

$$l_b = \frac{L_0}{\prod_{i=1}^q 2 \cos(\alpha_{i0})} = \frac{L}{\prod_{i=1}^q 2 \cos(\alpha_i)} \quad (10)$$

which leads to $L = L_0 \frac{\Xi}{\Xi_0}$. The change in the length of the D-Bar can be written as:

$$\Delta L = L_0 \left(\frac{\Xi}{\Xi_0} - 1 \right). \quad (11)$$

The relation between ΔS_q and l_b can be written as:

$$\Delta S_q = 2l_b(\sin(\alpha_q) - \sin(\alpha_{q0})) = \frac{2L_0}{\Xi_0}(\sin(\alpha_q) - \sin(\alpha_{q0})), \quad (12)$$

Substituting from Equations (11) and (12) into $G_1(q) = \frac{\Delta L}{\Delta S_q}$, we get back Equation (8). The same approach is followed to get Equation (9) for the geometrical relations of the 3D D-Bar. \square

Example 2: Consider a D-bar structure where $\forall \alpha_i = \alpha$, substituting α to α_i in Equation (8), we get:

$$G_1(q) = \frac{2^{q-1}(\cos^q \alpha - \cos^q(\alpha - h))}{\sin \alpha - \sin(\alpha - h)}, \quad (13)$$

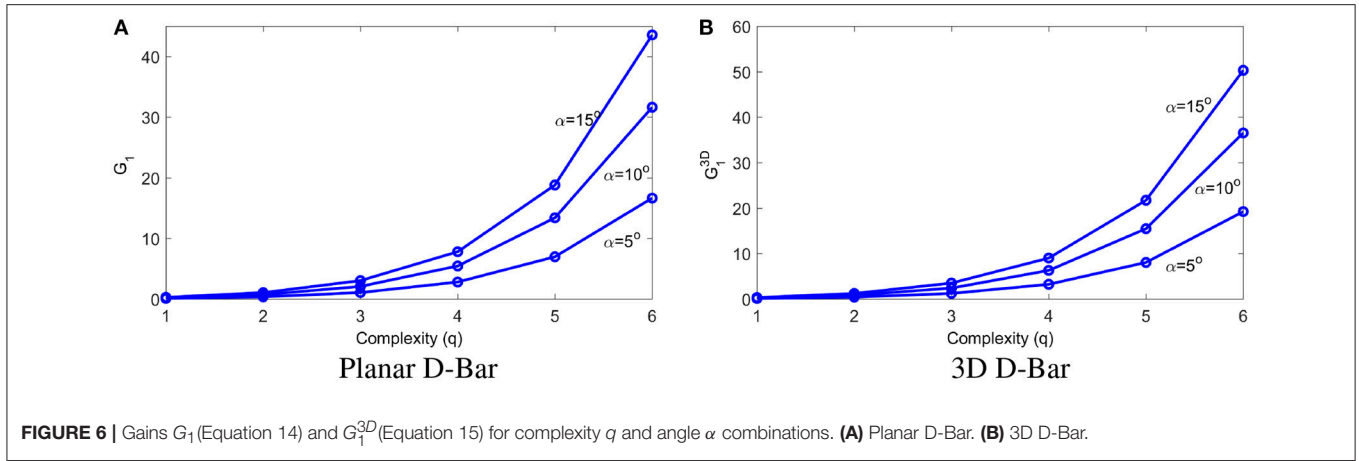
where $h = \alpha - \alpha_0$. Taking the limit as h approaches zero, Equation (13) yields:

$$G_1(q) \approx \lim_{h \rightarrow 0} G_1(q) = -2^{q-1} q \cos^{q-2} \alpha \sin \alpha. \quad (14)$$

Similarly, $G_1^{3D}(q)$ for $N = 3$, can be written as:

$$G_1^{3D}(q) \approx \frac{-2^{q-1} q \cos^{q-2} \alpha^{3D} \sin \alpha^{3D}}{\cos(\frac{\pi}{6})}. \quad (15)$$

Note that the $-$ sign in Equations (14) and (15) suggests that if length of the D-bar reduces, length of the string at complexity level q increases. **Figure 6** shows the magnitude of the gain $G_1(q)$ and $G_1^{3D}(q)$ for various angle and complexity configurations. The angle α is evaluated for the values of $5^\circ, 10^\circ,$ and 15° . From **Figure 6**, it is clear that the increasing complexity and increasing angle lead to higher ratios of ΔL and ΔS_q . To summarize, if the structure is employed for length related parametric



modifications, the angle and complexity should be selected as high as possible to relate the higher level of displacements to a smaller amount of length change for the strings at level q . This observation is valid for both planar and 3D versions with values of the $G_1^{3D}(q)$ being greater than the $G_1(q)$.

3.2. Force Gain : F/t_q

By tracking the tension over the strings of the D-Bar at higher complexities, it is possible to estimate the compressive force F . Therefore, it is possible to create a configuration with inherent force sensing properties. Furthermore, similar to the configuration for length gain, the sensing capability is robust to the structural failures within the D-Bar itself due to the presence of multiple members with the same contribution to the load-bearing configuration. In other words, the presence of multiple strings leads to a successful force sensor even when one or more strings malfunction. In addition, similar to the length gain, it is also possible to use the D-Bar as actuator governed by the same relations observed for the sensor.

Theorem 2: The Gain $G_2(q)$, defined as the ratio of the external force applied to the tension in the shortest string at complexity q level, is given by:

$$G_2(q) = \frac{F}{t_q} = \frac{\prod_{i=1}^q 2 \cos(\alpha_i)}{2 \sin(\alpha_q)}. \quad (16)$$

Extension of the planar relation to the 3D yields:

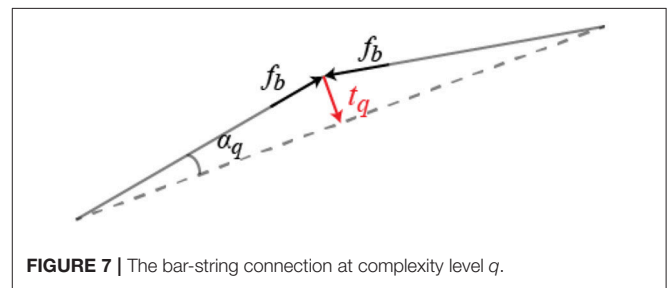
$$G_2^{3D}(q) = \frac{F}{t_q^{3D}} = \frac{(\prod_{i=1}^q N \cos(\alpha_i^{3D})) \cos(\frac{N\pi-2\pi}{2N})}{(\sin(\alpha_q^{3D}))}. \quad (17)$$

Proof: We can write the equation of static balance by looking at the node in **Figure 7** as:

$$t_q = 2f_b \sin(\alpha_q) \quad (18)$$

where f_b is force on the bar. The bar force is related to the compressive force F as:

$$f_b = \frac{F}{\prod_{i=1}^q 2 \cos(\alpha_i)}. \quad (19)$$



Combining Equations (18) and (19), Equation (16) is found. Adopting the same method, it is straightforward to derive the relation given in Equation (17). □

Example 3: In this example consider the special case of the D-Bar for both planar and 3D versions introduced in example 2. Substituting α to α_i in Equation (16) leads to the gain relation as:

$$G_2(q) = \frac{(2 \cos \alpha)^{q-1}}{\tan \alpha}. \quad (20)$$

For 3D configuration, the gain $G_2^{3D}(q)$ becomes:

$$G_2^{3D}(q) = \frac{F}{t_q^{3D}} = \frac{(3 \cos \alpha^{3D})^q \cos(\frac{N\pi-2\pi}{2N})}{(\sin(\alpha_q^{3D}))}. \quad (21)$$

Figure 8 shows the relation between the F and the t_q for both planar and 3D versions. From **Figure 8**, it is concluded that the value of the $G_2(q)$ increases with the increasing number of complexity q and decreases with the increasing angle of the D-bar angle α . It is also worth stating that the gains $G_1(q)$ and $G_2(q)$ show opposite behavior with respect to the D-bar angle α .

3.3. Length to Force Gain : $F/\Delta S_q$

Using the Hooke's law and the length changes over the strings of the D-Bar at higher complexities, it is possible to estimate the compressive force F . Therefore, it is possible to track the force change using the length changes over the strings of the sensor. Similar to the configuration for length gain and force gain, the sensor configuration is also robust to the structural failures.

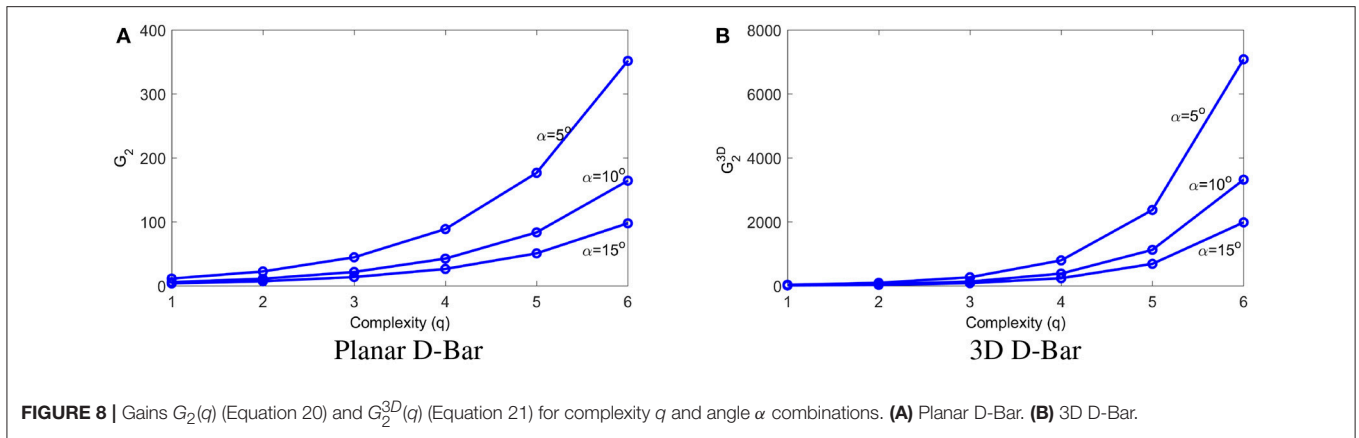


FIGURE 8 | Gains $G_2(q)$ (Equation 20) and $G_2^{3D}(q)$ (Equation 21) for complexity q and angle α combinations. **(A)** Planar D-Bar. **(B)** 3D D-Bar.

Lemma 1: Let the extensional stiffness k_q be given. The Force to Length Gain $G_3(q)$, defined as the ratio of the applied force to the change in length of the shortest string in a D-bar system of complexity q , is given by:

$$G_3(q) = \frac{F}{\Delta S_q} = k_q G_2(q). \tag{22}$$

The extension of the expression given in Equation (22) yields:

$$G_3^{3D}(q) = \frac{F}{\Delta S_q^{3D}} = k_q G_2^{3D}(q). \tag{23}$$

Proof: Using the assumption 2 and replacing the t_q with the expression $t_q = k_q \Delta S_q$ in Equation (16), it is straightforward to see the relation in Equation (22). The gain $G_3(q)$ is related to the gain $G_2(q)$ by the linear relationship $G_3(q) = k_q G_2(q)$. The relations between the $G_2^{3D}(q)$ and $G_3^{3D}(q)$ are exactly the same as explained for the planar configuration.

Example 4: This example presents a minimal mass sensor design. Consider the minimal mass formulation of the planar and 3D versions of D-Bar when $\forall \alpha_i = \alpha$ as given in Equations (4) and (6) where i denotes the each self-similar iteration such that $i = 1q$. The materials are selected as given in **Table 1**. Given the data: $L = 0.25m$, $\alpha = 10^\circ$, $F = 1000N$, we find $\epsilon = 0.0039$. The normalized mass of the structure vs. complexity q is shown in **Figure 9**.

Using the relation shown in Equation (6), it is possible to find the complexity at which yielding becomes the mode of failure. In this example, if the complexity q is greater than 3 for the planar configuration, yielding becomes the mode of failure. On the other hand, for the 3D configuration, the mode of failure becomes yielding when q is greater than 9. Such a difference is due to the fact that the 3D D-bar shares the compressive load with more members. In order to find the optimal complexity of the D-bar for the minimal mass configuration, the bar masses should be incorporated for yielding conditions after the corresponding complexity levels. The mass ratios given in Equations (4) and (5) are no longer valid if the yielding is the mode of failure. The

modified versions of the μ and μ_{3D}^N for yielding are given by:

$$\mu = \mu_{3D}^N = \frac{\tau}{\cos^q \alpha} + \epsilon (\cos^{-2q} \alpha - 1), \tag{24}$$

where τ is similar to ϵ and is given by:

$$\tau = \frac{\sqrt{\pi} \sqrt{E_b} \sqrt{F}}{2 \sigma_b L}, \tag{25}$$

where σ_b is the yield stress of the bar material.

Figures 9A,B show the normalized mass of the planar and 3D configurations. Optimal complexity in terms of minimal mass is achieved when $q = 4$ for the planar D-Bar and $q = 10$ for the 3D D-Bar. For those complexities normalized mass ratios μ and μ_{3D} become 0.30 and 0.36, corresponding to a mass savings of 70% and 64%, respectively. For the selected α and the complexities of the two configurations the gain $G_1(q)$ becomes $G_1(4) = -5$. Evaluation of the $G_2(q)$ yields the value of $G_2(4) = 43$. If the gains for the 3D version are evaluated the resultant value of the gains become $G_1^{3D}(10) = -908$ and $G_2^{3D}(10) = 25 \times 10^4$. For $G_3(q)$ we need to have the string stiffness k_q at the complexity level q . The length of the string at the complexity level i for a planar D-Bar is given by:

$$S_i = \frac{2L \sin \alpha}{(2 \cos \alpha)^i}. \tag{26}$$

The stiffness of the string on complexity level i can be calculated as:

$$k_i = \frac{E_s A_i}{S_i}, \tag{27}$$

where E_s is the elastic modulus of the strings at complexity level i , and A_i is the cross sectional area of the string. Substituting for $A_i = \frac{t_i}{\sigma_y}$ and $t_i = F \frac{(2 \cos \alpha)^{i-1}}{\tan \alpha}$ leads to:

$$k_i = \frac{E_s F}{L \sigma_y}. \tag{28}$$

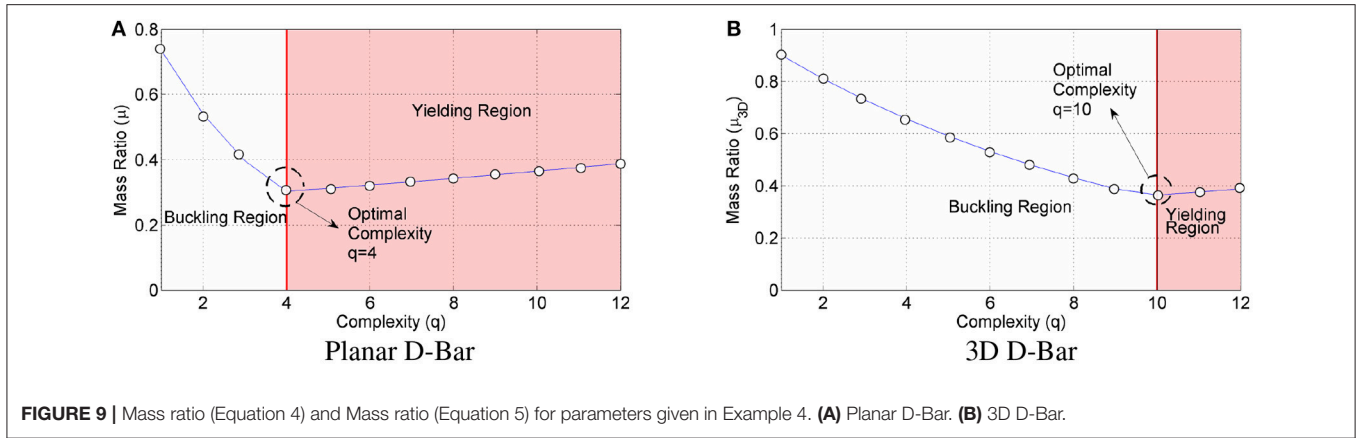


FIGURE 9 | Mass ratio (Equation 4) and Mass ratio (Equation 5) for parameters given in Example 4. **(A)** Planar D-Bar. **(B)** 3D D-Bar.

Equation (28) indicates that the minimal mass planar D-Bar has the same string stiffness for every complexity level i . Then, the $G_3(q)$ can be written as:

$$G_3(q) = \frac{E_s F G_2}{L \sigma_y} = 7700 N/mm. \quad (29)$$

Now for the evaluation of the gain $G_3^{3D}(q)$, the string stiffness for the complexity q must be known. The string stiffness of the 3D D-Bar when $\forall \alpha_i^{3D} = \alpha^{3D}$, and the string length for any complexity q becomes:

$$S^{3D}(q) = \frac{2L \sin \alpha^{3D} \cos\left(\frac{N\pi - 2\pi}{2N}\right)}{(2 \cos \alpha^{3D})^q}. \quad (30)$$

Recalling the relation $A_q^{3D} = t_q^{3D} / \sigma_y$ and replacing the t_q^{3D} as:

$$t_q^{3D} = \frac{F \sin \alpha}{(N \cos \alpha^{3D})^q \cos\left(\frac{N\pi - 2\pi}{2N}\right)}, \quad (31)$$

the cross sectional area of the string A_i^{3D} becomes:

$$A_q^{3D} = \frac{F \sin \alpha^{3D}}{(N \cos \alpha^{3D})^q \cos\left(\frac{N\pi - 2\pi}{2N}\right) \sigma_y}. \quad (32)$$

Combining all of those expressions give the stiffness of a string at the complexity level i as:

$$k_q^{3D} = \left(\frac{2}{N}\right)^q \frac{E_s F}{2L \sigma_y \cos^2\left(\frac{N\pi - 2\pi}{2N}\right)}. \quad (33)$$

Using the definition of the $G_3^{3D}(q) = k_q^{3D} G_2^{3D}(q)$ and $N = 3$, we get $G_3^{3D}(q) = 16.4 \times 10^6 N/mm$.

4. STIFFNESS CALCULATION OF THE D-BAR

It is useful to quantify stiffness of a structure for a given configuration. For this purpose, the compressive stiffness of the

D-bar is calculated. We will define stiffness as the second partial derivative of the potential energy stored in the structure with respect to its length, that is:

$$K = \frac{\partial^2 PE}{\partial L^2}. \quad (34)$$

4.1. Stiffness of the Planar D-Bar

The number of strings in complexity i for a planar D-Bar is given by $n_s = 2^{2i-2}$. As bars are rigid, strings are the only elements of the structure which can store energy. The length of a string at complexity level i is given as (Skelton and de Oliveira, 2009) :

$$s_i = \frac{2L \sin(\alpha_i)}{\prod_{n=1}^i 2 \cos(\alpha_n)}, \quad (35)$$

the PE can be written as the sum of energy stored in individual strings as:

$$PE = \sum_{i=1}^q \frac{1}{2} n_s k_i (s_i - s_0)^2 \quad (36)$$

Substituting for n_s and s_i from above gives the equation for PE as:

$$PE = \sum_{i=1}^q 2^{2i-3} k_i \left[\frac{2L \sin(\alpha_i)}{\prod_{n=1}^i 2 \cos(\alpha_n)} - s_0 \right]^2. \quad (37)$$

Lemma 2: If all of the D-bar angles α for any given complexity q are equal, ($\forall \alpha_i = \alpha$), then the stiffness formulation becomes:

$$K = \frac{1}{q^2} \sum_{i=1}^q k_i \csc^2 \alpha \cos^q \alpha_0 \cos^{-2i-q} \alpha \left[\csc \alpha (\cos^4 \alpha [q - iq + i^2 - 2i + 1] + \cos^2 \alpha [-2i^2 + 2iq + 2i - q - 2] + i^2 - iq) \left(\sin \alpha \left(\frac{\cos \alpha}{\cos \alpha_0} \right)^q - \sin \alpha_0 \left(\frac{\cos \alpha}{\cos \alpha_0} \right)^i \right) + (\cos^2 \alpha [i - q - 1] - i + q)^2 \left(\frac{\cos \alpha}{\cos \alpha_0} \right)^q \right]. \quad (38)$$

where α is the angle of the D-bar, α_0 is the angle of the D-bar when there is no application of the force, k_i is the stiffness of the

individual strings at complexity level i .

Proof: If we recall Equation (37) and replace all of the α_i with α , the potential energy equation becomes:

$$PE = \sum_{i=1}^q 2^{2i-3} k_i \left(\frac{2L \sin \alpha}{(2 \cos \alpha)^i} - s_0 \right)^2. \quad (39)$$

Using the relation between L and bar length l_b , we get:

$$PE = \sum_{i=1}^q 2^{2i-3} k_i (2l_b (2 \cos \alpha)^{(q-i)} \sin \alpha - s_0)^2, \quad (40)$$

and then substituting for $\cos \alpha$ and $\sin \alpha$ as:

$$\cos \alpha = \frac{1}{2} \left(\frac{L}{l_b} \right)^{1/q}, \quad \sin \alpha = \sqrt{1 - \frac{1}{4} \left(\frac{L}{l_b} \right)^{2/q}}, \quad (41)$$

we get:

$$PE = \sum_{i=1}^q 2^{2i-3} k_i \left[2l_b \left(1 - \frac{1}{4} \left(\frac{L}{l_b} \right)^{2/q} \right)^{\frac{1}{2}} \left(\frac{L}{l_b} \right)^{\frac{q-i}{q}} - s_0 \right]^2. \quad (42)$$

Notice that PE is a function of the structural parameter L . If we take the second partial derivative of the potential energy with respect to L and substitute the relations $L = l_b (2 \cos \alpha)^q$ and $s_{0i} = 2l_b \sin \alpha_0 (2 \cos \alpha_0)^{q-i}$ back to the final expression, we get Equation (38). \square

It is possible to approximate Equation (38) by assuming that the D-bar operates around $\alpha \approx \alpha_0$. For this we replace $\alpha_0 = \alpha - h$. Then, Equation (38) becomes:

$$K = \lim_{h \rightarrow 0} \left[\frac{1}{q^2} \sum_{i=1}^q k_i \csc^2 \alpha \cos^q(\alpha - h) \cos^{-2i-q} \alpha \left[\csc \alpha \left(\cos^4 \alpha [q - iq + i^2 - 2i + 1] + \cos^2 \alpha [-2i^2 + 2iq + 2i - q - 2] + i^2 - iq \right) \left(\frac{\cos \alpha}{\cos(\alpha - h)} \right)^q - \sin(\alpha - h) \left(\frac{\cos \alpha}{\cos(\alpha - h)} \right)^i \right. \right. \\ \left. \left. + (\cos^2 \alpha [i - q - 1] - i + q)^2 \left(\frac{\cos \alpha}{\cos(\alpha - h)} \right)^q \right] \right]. \quad (43)$$

The stiffness of the structure K , as h approaches zero, becomes:

$$K = \frac{1}{q^2} \sum_{i=1}^q k_i \csc^2 \alpha \cos^{-2i} \alpha [(\cos^2 \alpha [i - q - 1] - i + q)^2]. \quad (44)$$

Choosing the stiffness value of the strings at each complexity i as equal (minimal mass case, as proved above) yields the stiffness as:

$$K = k \frac{\cot^2 \alpha \csc^2 \alpha (\sec^{2q} \alpha - 1) - q^2}{q^2} \quad (45)$$

4.2. Stiffness of the 3D D-Bar

It is straightforward to extend the stiffness calculation to the 3D D-Bar version. The number of strings in a 3D D-bar for each complexity level i are $n_s^N = N^i 2^{i-1}$. The length of a string at complexity level i for a 3D D-Bar is given as (Skelton and de Oliveira, 2009) :

$$s_i^{3D} = \frac{2L \sin(\alpha_i)}{\prod_{n=1}^i 2 \cos(\alpha_n)} \cos \left(\frac{N\pi - 2}{2N} \right), \quad (46)$$

the PE can be written as the sum of energy stored in individual strings as:

$$PE = \sum_{i=1}^q \frac{1}{2} n_s^N k_i (s_i^{3D} - s_0)^2 \quad (47)$$

Substituting for n_s^N and s_i^{3D} from above gives the equation for PE^{3D} as:

$$PE^{3D} = \sum_{i=1}^q N^i 2^{i-2} k_i \left[\frac{2L \sin(\alpha_i)}{\prod_{n=1}^i 2 \cos(\alpha_n)} \cos \left(\frac{N\pi - 2}{2N} \right) - s_{0i} \right]^2. \quad (48)$$

Substituting for s_{0i} in Equation (48) leads to:

$$PE^{3D} = \sum_{i=1}^q N^i 2^{i-2} k_i \left[\frac{2L \sin(\alpha_i)}{\prod_{n=1}^i 2 \cos(\alpha_n)} \cos \left(\frac{N\pi - 2\pi}{2N} \right) - \frac{2L_0 \sin(\alpha_{i0})}{\prod_{n=1}^i 2 \cos(\alpha_{n0})} \cos \left(\frac{N\pi - 2\pi}{2N} \right) \right]^2. \quad (49)$$

The potential energy stored on complexity level i can be written as:

$$PE_i^{3D} = \left(\frac{N}{2} \right)^i \cos^2 \left(\frac{N\pi - 2\pi}{2N} \right) PE_i^{2D}. \quad (50)$$

Adding potential energies on all complexity levels, we get:

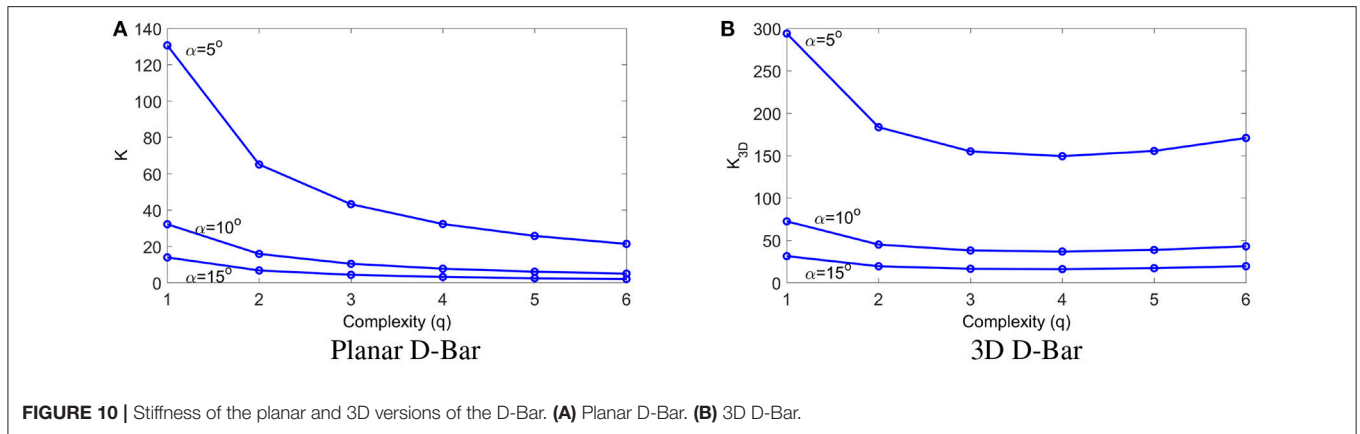
$$PE^{3D} = 2 \cos^2 \left(\frac{N\pi - 2\pi}{2N} \right) \sum_{i=1}^q \left(\frac{N}{2} \right)^i PE_i^{2D}. \quad (51)$$

Selecting all angles of the D-Bar to be equal and adopt the method presented for planar D-Bar, the relation presented in Equation (51) reduces to:

$$K_{3D} = \frac{2}{q^2} \cos^2 \left(\frac{N\pi - 2\pi}{2N} \right) \sum_{i=1}^q \left(\frac{N}{2} \right)^i k_i \csc^2 \alpha \cos^{-2i} \alpha [(\cos^2 \alpha [i - q - 1] - i + q)^2]. \quad (52)$$

Example 5: In this example, the stiffness of the planar and 3D tensegrity D-Bar configurations are evaluated for various angle and complexity combinations. Assuming that all the strings have unit stiffness $k_i = 1$ and $N = 3$, the variation in the stiffness of the structure is shown in **Figure 10**.

From **Figure 10A**, it can be seen that the stiffness of the planar D-Bar increases as the complexity, q , and angle α decreases. This



is reasonable since as the angle and complexity decreases, the bars participate more and more in the load bearing. Thus the rigidity of the bars increases the stiffness of the structure in the horizontal direction.

From **Figure 10B**, similar to the planar D-Bar, the stiffness of the 3D configuration increases as angle α decreases. However, in contrast to the planar D-bar, the stiffness K of the structure decreases for the first few self-similar iterations then starts to increase again. Such behavior difference is due to the number of the strings added to the structure. In contrast to the planar tensegrity structure, the number of the strings in the 3D case increases as $\left(\frac{3}{2}\right)^i$ times more for each iteration step compared to the planar D-Bar.

Example 6: In this example, we calculate the stiffness values of the planar and 3D D-Bar structures presented in example 4. The stiffness of a string is given by Equation (28). If all the parameters given in example 4 are substituted back to Equation (28), the stiffness of one string is found as $k = 177N/mm$. Given the minimal mass design $q = 4$ and $\alpha = 10^\circ$ with $\mu = 0.30$, the value of the K is found as $1366N/mm$. Evaluation of the K_{3D} is also similar to the planar configuration. The string stiffnesses for the 3D D-Bar are calculated by substituting i instead of q for each complexity level i and substituting k_i in Equation (52), we get:

$$K_{3D} = \frac{E_s F [\cot^2 \alpha \csc^2 \alpha (\sec^{2q} \alpha - 1) - q^2]}{L \sigma_y q^2} \quad (53)$$

Substituting for the force $F = 1000N$, $\alpha = 10^\circ$, $L = 0.25m$, and minimal mass complexity $q = 10$ where $\mu_{3D} = 0.36$, the resultant stiffness becomes $K = 501N/mm$. The minimal mass planar D-Bar has 3 times the stiffness of the minimal mass 3D D-Bar.

Lemma 3: Let angle α and complexity q be equal for planar and 3D D-Bar. The minimum mass design of the planar and 3D D-Bars lead to same global stiffnesses K and K_{3D} formulated as:

$$K = K_{3D} = \frac{E_s F [\cot^2 \alpha \csc^2 \alpha (\sec^{2q} \alpha - 1) - q^2]}{L \sigma_y q^2} \quad (54)$$

Proof: Equation (53) gives the global stiffness K_{3D} of the 3D D-Bar. Recalling the global stiffness formula given in Equation (45)

and substituting the individual string stiffness k with the minimal string stiffness given in Equation (28) expression presented in Equation (54) is found. This concludes the proof.

5. MASS OF THE D-BAR SUBJECT TO STIFFNESS CONSTRAINT

In this section, mass calculation of the planar D-bar subject to stiffness requirement, when $\forall \alpha_i = \alpha$ and $\forall k_i = k$, is presented. The mass of a string at complexity level i is given by:

$$m_i = \rho_s A_i s_i = \frac{\rho_s s_i^2 k}{E_s} \quad (55)$$

where cross sectional area $A_i = \frac{s_i k}{E_s}$ and E_s is the elastic modulus of the string material. From Equation (45), we can write:

$$m_i = \frac{\rho_s s_i^2 K q^2}{E_s [\cot^2 \alpha \csc^2 \alpha (\sec^{2q} \alpha - 1) - q^2]} \quad (56)$$

Thus, total string mass m_{st} can be written as:

$$m_{st} = \sum_{i=1}^q 4^{i-1} m_i = \frac{\rho_s K q^2 L^2 (\sec^{2q} \alpha - 1)}{E_s [\cot^2 \alpha \csc^2 \alpha (\sec^{2q} \alpha - 1) - q^2]} \quad (57)$$

The bar masses should be calculated by checking the primary mode of failure. Inequality (6) is used to evaluate if buckling or yielding is the primary mode of failure. Equations (58) and (59) present mass of the bars for buckling condition and yielding condition, respectively.

$$m_{bar} = \frac{2 \rho_b L^2}{2^{\frac{q}{2}} \cos^{\frac{5q}{2}} \alpha} \sqrt{\frac{F}{E_b \pi}} \quad (58)$$

$$m_{bar} = \frac{\rho_b FL}{\sigma_b \cos^{2q} \alpha} \quad (59)$$

The total mass of the structure is given as $m = m_{bar} + m_{st}$.

TABLE 2 | Mass of the D-Bar satisfying $K = 500N/mm$.

Complexity	Angle(α)	Bar failure	Total mass
$q = 1$	No solution	No solution	No solution
$q = 2$	22.14°	Buckle	16.8 gm
$q = 3$	18.16°	Buckle	11.9 gm
$q = 4$	15.77°	Buckle	8.45 gm
$q = 5$	14.12°	Yield	8.37 gm
$q = 6$	12.91°	Yield	8.37 gm
$q = 7$	11.95°	Yield	8.37 gm

Example 7: This example shows a procedure to design a minimal mass planar D-Bar for a fixed global stiffness $K = 500N/mm$. The materials, force, and size are picked exactly as given in example 4.

Equation (28) gives the minimum stiffness, k_{min} of strings to avoid yielding. To find the minimal mass solution to satisfy the required K value a search algorithm is summarized below.

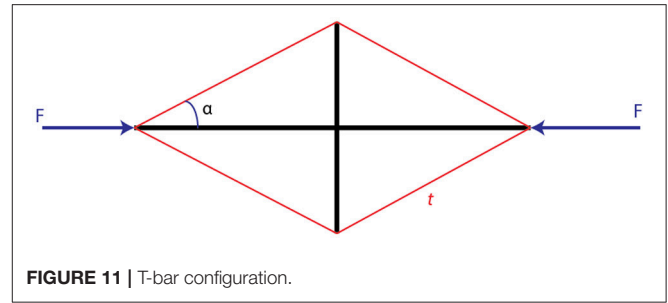
We start with complexity one and search for all the α values in small increment till $\alpha = 29.477^\circ$. We choose the angle to get closest possible $k \geq k_{min}$ to get the string mass and check for the failure mode for bars and design them accordingly. We repeat the procedure for the higher complexities till we get the minimum possible mass.

Table 2 gives the complexity, corresponding angle, mode of failure and the mass of the D-Bar which satisfies the desired global stiffness value $K = 500N/mm$. We observe that the primary mode of failure changes from buckling to yielding after complexity $q = 4$. The minimum mass design is complexity $q = 5$ with an angle of $\alpha = 14.12^\circ$.

6. COMBINATION OF PLANAR T-BAR AND D-BAR

Applications of the D-Bar can be extended by combining the D-Bar with other tensegrity structures such as T-Bar. T-Bar offers better mass efficiency than the D-Bar (Skelton and de Oliveira, 2009) and D-bar provides deployability. Hence by combining the D-Bar and T-Bar, it is possible to generate a tensegrity configuration where T-Bar contributes to the mass efficiency and D-Bar contributes to deployability. **Figure 11** shows a T-bar under compressive load. This structure has proven to be more mass efficient than D-bar (Skelton and de Oliveira, 2009). The strings in T-bar structure are prestressed to avoid global buckling.

Self-similarity can also be used for T-bars to minimize the mass. If the self-similarity approach is implemented n times, and at the n th iteration instead of the T-Bar, a D-bar unit is used for the self-similar step, the new structure would have complexity $q = n + 1$ with n level of T-bar units and 1 level of D-bar unit. We name such structure as T_nD_1 Bar which combines the mass efficiency of T-Bar with the deployability of D-Bar. **Figure 12** shows the structural configuration for complexity 4, T_3D_1 Bar structure with T-Bar angle of α_{ti} for



each complexity level of $i = 1$ to n and the D-Bar angle of the α_d .

For the T_nD_1 Bar, the serially connected D-Bars are the structural members which resist the compressive loading and the strings inherited from the T-Bar iterations provide global stiffness to the structure.

The structure under the compressive loading is, in fact, nothing but a 2^n complexity 1 D-Bar units connected in series and the vertical bars of the T-Bar fractals support the connection between two serially connected D-Bars. Following the approach presented in Skelton and de Oliveira (2009), the minimal mass formulation of the T_nD_1 bar under the buckling condition becomes:

$$\mu^{TD} = \sum_{i=1}^n \left(\frac{\tan^{5/2} \alpha_{ti}}{2^i} + \epsilon(1 + \tan^2 \alpha_{ti}) \right) + \epsilon \tan^2 \alpha_d + \frac{1}{2^{n+1/2} \cos^{5/2} \alpha_d} \tag{60}$$

where ϵ is defined in Equation (2) and if $\forall \alpha_{ti} = \alpha_t$, then Equation (60) gives:

$$\mu^{TD} = \frac{2^n - 1}{2^n} \tan^{5/2} \alpha_t + n\epsilon(1 + \tan^2 \alpha_t) + \epsilon \tan^2 \alpha_d + \frac{1}{2^{n+1/2} \cos^{5/2} \alpha_d} \tag{61}$$

As explained in section 2, the primary mode of the failure for the minimal mass design should be checked as the number of self-similar iterations increase. With a simple modification of Equation (6), the condition from buckling to yielding failure for the D-Bars of the T_nD_1 is found as:

$$\frac{F}{L^2} > \frac{4\sigma_b^2}{2^{2n+1} \pi E_b \cos \alpha_d} \tag{62}$$

The same condition for the vertical bars of T_nD_1 configuration at the i th complexity level is given as:

$$\frac{F}{L^2} > \frac{\sigma_b^2 \tan \alpha_{ti}}{2^{2i-2} \pi E_b} \tag{63}$$

If the failure mode of the bars become yielding, the normalized mass ratio (μ^{TD}) given in Equations (60) and (61) are no longer

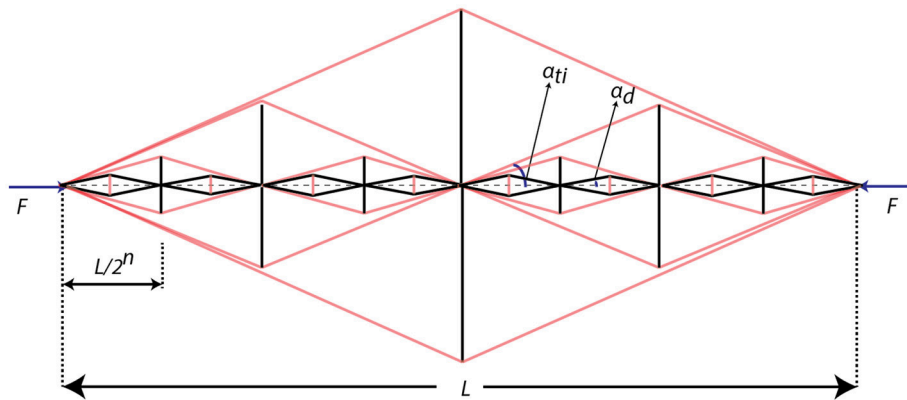


FIGURE 12 | TD-bar configuration.

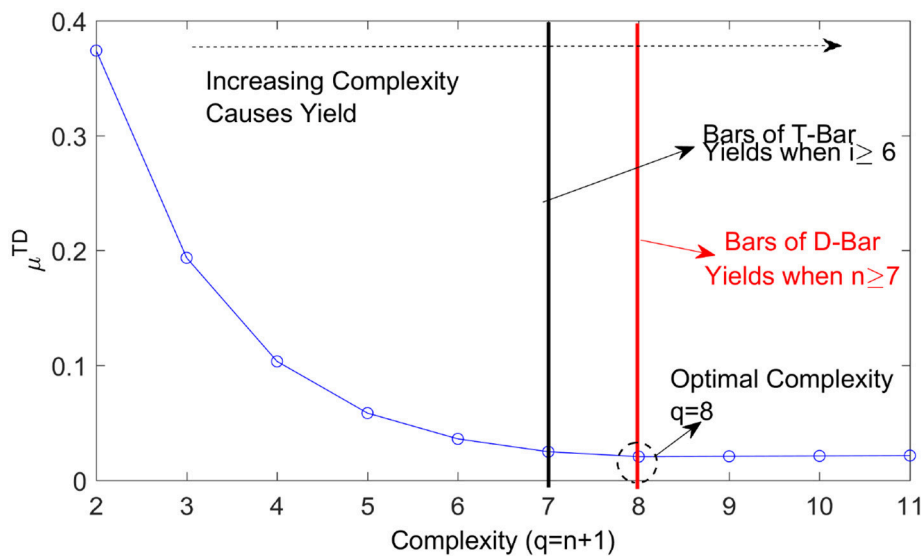


FIGURE 13 | Mass ratio of the configuration vs. the complexity of the structure.

valid. Let i_y represent the complexity level of the T – Bar fractals for which vertical bars yield and let q_y represent the complexity where bars of the D-Bars yield. For a given complexity q , if $q < q_y$ but $q \geq i_y + 1$, the mass ratio becomes:

$$\mu^{TD} = \sum_{i=1}^{i_y-1} \left(\frac{\tan^{5/2} \alpha_{ti}}{2^i} \right) + \tau \sum_{j=i_y}^n \tan^2 \alpha_{tj} + \sum_{i=1}^n \epsilon (1 + \tan^2 \alpha_{ti}) + \epsilon \tan^2 \alpha_d + \frac{1}{2^{n+\frac{1}{2}} \cos^{\frac{5}{2}} \alpha_d}. \quad (64)$$

In addition, if $q > q_y$, the normalized mass ratio becomes:

$$\mu^{TD} = \sum_{i=1}^{i_y-1} \left(\frac{\tan^{5/2} \alpha_{ti}}{2^i} \right) + \tau \sum_{j=i_y}^n \tan^2 \alpha_{tj} + \sum_{i=1}^n \epsilon (1 + \tan^2 \alpha_{ti}) + \epsilon \tan^2 \alpha_d + \tau \frac{1}{\cos^2 \alpha_d}. \quad (65)$$

Similarly, $\forall \alpha_{ti} = \alpha_t$, Equations (64) and (65) give:

$$\mu^{TD} = \frac{2^{i_y} - 2}{2^{i_y}} \tan^{\frac{5}{2}} \alpha_t + (n - i_y + 1) \tau \tan^2 \alpha_t + n \epsilon (1 + \tan^2 \alpha_t) + \epsilon \tan^2 \alpha_d + \frac{1}{2^{n+\frac{1}{2}} \cos^{\frac{5}{2}} \alpha_d}, \quad (66)$$

$$\mu^{TD} = \frac{2^{i_y} - 2}{2^{i_y}} \tan^{\frac{5}{2}} \alpha_t + (n - i_y + 1) \tau \tan^2 \alpha_t + n \epsilon (1 + \tan^2 \alpha_t) + \epsilon \tan^2 \alpha_d + \tau \frac{1}{\cos^2 \alpha_d}. \quad (67)$$

Practical design of the 3D TD-Bar requires delicate handling of the angles of self-similar T-Bar and D-Bar components due to the possibility of entanglement. This can be avoided by setting the angles at each self-similar level strictly less or equal to that of the previous self-similar iterations at the cost of minimum mass.

Example 8: Consider a $T_n D_1$ bar which has a length of $L = 10m$, angles of $\forall \alpha_{ti} = \alpha_d = 10^\circ$ and a compressive load

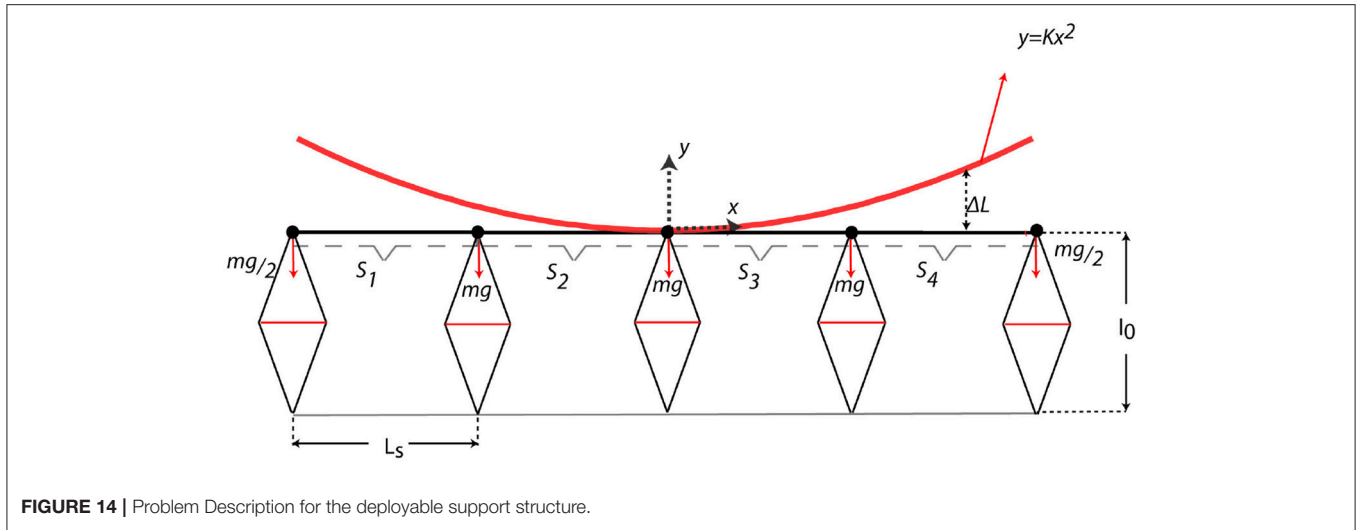


FIGURE 14 | Problem Description for the deployable support structure.

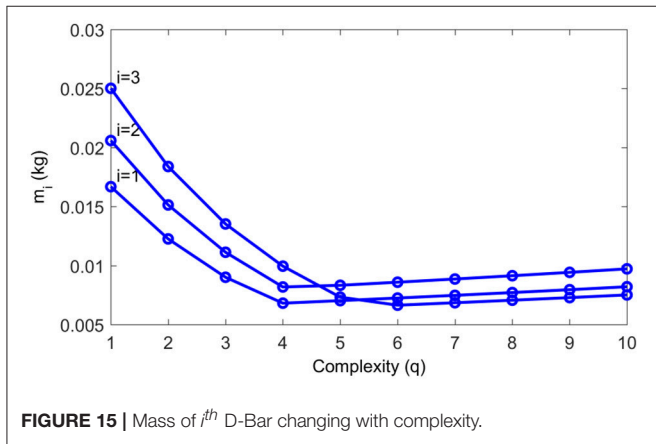


FIGURE 15 | Mass of i^{th} D-Bar changing with complexity.

TABLE 3 | Optimal Complexities (q_i), angles(α_{0i}), and masses(m_i) of i^{th} D-Bar.

	$i = 1$	$i = 2$	$i = 3$
q_i	4	4	6
α_{0i}	10°	15.3°	20.2°
$m_i(kg)$	6.8×10^{-3}	8.2×10^{-3}	6.5×10^{-3}

Equation (71) is the equivalent stiffness of the 2^n serially connected D-Bars with the approximated stiffness formulation derived in Equation (45).

It is possible to simplify G_1^{TD} further if $\alpha_d \approx \alpha_{d0}$. Using the procedure described in section 4 for $\alpha_d = \alpha_{d0} + h$, the G_1^{TD} reduces to

$$G_1^{TD} = -2^n \tan \alpha_d. \tag{72}$$

Example 9: For the $T_n D_1$ bar designed in example 8, the gains are $G_1^{TD} = -22.5$ and G_2^{TD} is 5.6. For the G_3^{TD} calculation the stiffness of the string, k_d must be known. Adopting the similar approach as presented for the derivation of Equation (28), k_d is given by:

$$k_d = 2^n \frac{E_s F}{L \sigma_y}, \tag{73}$$

and for this example, it takes the value of $k_d = 569N/mm$ leading to $G_3^{TD} = 3226N/mm$. Stiffness of the $T_n D_1$ bar is also calculated as $K_{TD} = 143N/mm$.

7. DESIGNING A MINIMAL MASS LOADED PLATFORM TO DEPLOY TO A SPECIFIED SHAPE AND STIFFNESS

Consider a deployable support structure composed of D-Bars to orient a host with 4 different segments, S_1, S_2, S_3 , and S_4 as depicted in Figure 14. In this example, there are 5 discrete

of $F = 1000N$. The materials are selected as given in Table 1. Figure 13 shows the mass ratio of the configuration as the complexity of the structure increases.

Two vertical lines in the graph represent the change in the primary mode of failure from buckling to yielding. As shown in the figure above $T_7 D_1$ turned out to be the optimum mass configuration for the given load and length of the structure.

Besides the normalized mass ratio, the gain relations described in section 2 are modified for $T_n D_1$ bar as:

$$G_1^{TD} = 2^n \frac{\cos \alpha_d - \cos \alpha_{d0}}{\sin \alpha_d - \sin \alpha_{d0}}, \tag{68}$$

$$G_2^{TD} = \frac{1}{\tan \alpha_d}, \tag{69}$$

$$G_3^{TD} = \frac{k_d}{\tan \alpha_d}. \tag{70}$$

Furthermore, the stiffness of the $T_n D_1$ bar is also given as

$$K_{TD} \approx \frac{k_d}{2^n \tan^2 \alpha_d}. \tag{71}$$

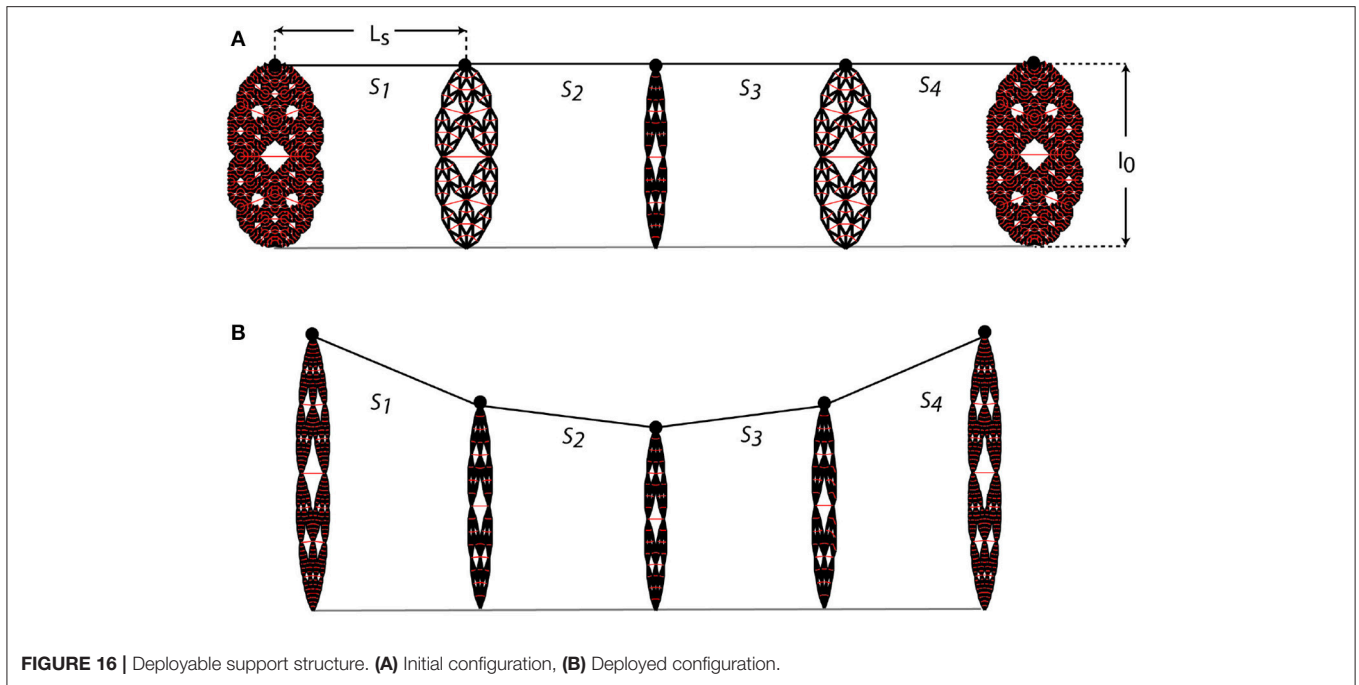


FIGURE 16 | Deployable support structure. (A) Initial configuration, (B) Deployed configuration.

segments and 5 D-Bars are used to support and orient them. Each segment has a mass of $m = 100\text{kg}$ and a length of $L_s = 0.25\text{m}$. The initial length l_0 of all D-Bars are equal to 0.25m as shown in Figure 14. The materials selected are as given in Table 1.

When the final configuration is achieved by deploying all the D-Bars to their desired positions, the angle α of all D-Bars are 10° . When deployed, edges of each segment are required to trace the curve $y = Kx^2$. The origin of the coordinate system is chosen as the symmetry axis of the parabolic surface function and the weights of each segment are shared by D-Bars attached to their edges. The purpose is to minimize the masses of the all D-Bars considering the weight of the platform and design them to generate enough ΔL to satisfy the final shape requirement.

Section 2 shows the mass ratio μ for the minimal mass D-Bar for buckling condition. In this example, each D-Bar would have their own optimal configuration in terms of mass efficiency to satisfy the extension requirement ΔL . Thus, the complexities and angles of each D-Bar may be different. The symmetry of the structure allows to focus on the design of D-Bars for one half and extend the analysis to cover the whole. Thus, by defining a queue number i where i is 1 at the center and goes to $i = 3$ at the corner, minimal mass of a D-Bar satisfying buckling constraint is given by:

$$m_b^i = \frac{2l_0^2 \rho_b}{(2 \cos^5 \alpha_0)^{\frac{q_i}{2}}} \sqrt{\frac{F_i}{\pi E_b}} + \frac{\rho_s}{\sigma_s} F_i l_0 (\cos^{-2q_i} \alpha_{0i} - 1). \quad (74)$$

If the bar lengths get small and yielding becomes the primary mode of failure, then the mass of D-Bar becomes:

$$m_y^i = \frac{\rho_b}{\sigma_b} F_i l_0 (\cos^{-2q_i} \alpha_{0i}) + \frac{\rho_s}{\sigma_s} F_i l_0 (\cos^{-2q_i} \alpha_{0i} - 1), \quad (75)$$

where angle α_{0i} is the initial angle of the i th D-Bar. Using the geometrical relations, it is possible to relate $\cos \alpha_{0i}$ to final desired configuration angle α as:

$$\cos \alpha_{0i} = \left(\frac{l_0}{\Delta L_i + l_0} \right)^{\frac{1}{q_i}} \cos \alpha. \quad (76)$$

The ΔL_i in Equation (76) is the length change requirement on the i th D-Bar and is a function of the corresponding x_i coordinate. Since the length L_s should be conserved, the x_i of the i th D-Bar becomes the real positive root of the following polynomial satisfying the inequality $x_i > x_{i-1}$:

$$x_i^4 + \left(\frac{1 - 2K^2 x_{i-1}^2}{K^2} \right) x_i^2 - \left(\frac{2x_{i-1}}{K^2} \right) x_i + \left(\frac{x_{i-1}^2 + K^2 x_{i-1}^4 - L_s^2}{K^2} \right) = 0. \quad (77)$$

After the x_i for the i th D-Bar is substituted to the parabolic shape equation $y = Kx^2$, the ΔL_i of the i th D-Bar becomes $\Delta L_i = Kx_i^2$. Substituting Equation (76) back to Equations (74) and (75), we get:

$$m_b^i = \frac{2l_0^2 \rho_b}{(2 \cos^5 \alpha)^{\frac{q_i}{2}}} \sqrt{\frac{F_i}{\pi E_b}} \left(\frac{\Delta L_i + l_0}{l_0} \right)^{5/2} + \frac{\rho_s}{\sigma_s} F_i l_0 \left[\cos^{-2q_i} \alpha \left(\frac{\Delta L_i + l_0}{l_0} \right)^2 - 1 \right], \quad (78)$$

$$m_y^i = \frac{\rho_b}{\sigma_b} F_i l_0 (\cos^{-2q_i} \alpha) \left(\frac{\Delta L_i + l_0}{l_0} \right)^2 + \frac{\rho_s}{\sigma_s} F_i l_0 \left[\cos^{-2q_i} \alpha \left(\frac{\Delta L_i + l_0}{l_0} \right)^2 - 1 \right]. \quad (79)$$

TABLE 4 | Values of the gains and stiffness of the D-Bars for initial and final configurations.

		G_1	G_2	G_3 (N/mm)	K (N/mm)
Initial	$i = 1$	-5.4	43.3	7,560	1,340
	$i = 2$	-7.8	26.1	4,570	524
	$i = 3$	-51.4	63.1	5,500	83
Final	$i = 1$	-5.4	43.3	7,560	1,340
	$i = 2$	-5.4	43.3	7,560	1,340
	$i = 3$	-31.36	168.1	14,660	433

Total mass of all the D-Bars is found as

$$m = 2 \sum_{i=1}^3 \max(m_b^i, m_y^i) - \max(m_b^1, m_y^1) \quad (80)$$

Substituting for $K = 0.35$ and $i = 1, 2$, and 3 , the masses of each individual D-Bar are evaluated for the complexity span between $q = 1 \dots 10$. **Figure 15** shows the variation in mass of each individual D-Bar with increasing complexity.

From **Figure 15**, the optimal complexities for the 1st and 2nd D-Bars are same whereas the optimal complexity of the 3rd D-Bar is higher. Please note that the mass values are not same for the same complexity D-Bars because of the different α_{0i} . The optimal complexities, angles and the masses of each D-Bar are shown in the **Table 3**.

Note that as the D-Bar is located toward the edge, the angles of the initial position becomes higher and higher. This is due to the fact that, as previously described in the theorem 1, the longer length changes require higher values of initial angles. The total mass using the formula given in Equation (80) becomes 36.2 grams. **Figure 16** shows the final configuration of the structure after the D-Bars generate ΔL .

The gain and stiffness values of the D-Bars supporting the structure are calculated for the angle and complexity information given in **Table 3**. **Table 4** shows those values for the initial and final configurations of i th D-Bar.

It should be noticed from **Table 4** that since there is no deformation on the D-Bar at the center, it will keep its gain relations and stiffness constant. The gain and stiffness change between initial and final configurations gets higher as the D-Bar gets closer to the edges. This is due to increasing angular change during deployment. As explained before, the gains and stiffness values are nonlinear functions of the complexity and angles. Thus, during the design phase, if gains and stiffness values should have a specific value or range, careful evaluation of the problem to satisfy such requirements is necessary.

8. DISCUSSION AND CONCLUSION

This paper designs tensegrity D-Bar systems that can serve either of these functions: (i) sensors to measure displacements, (ii)

sensors to measure force, (iii) actuators to control displacement, (iv) actuators to control force applied, (v) minimal mass compressive structures subject to a stiffness requirement, and (vi) deployable structures that are efficient in compressive loads. To facilitate such designs, new analytical formulas are derived to give the system a specified displacement gain or force gain, or stiffness requirement.

First, an approach is developed to use the D-Bar for sensing applications. In this case, three different gain relations between the environment and the structural parameters are defined. It is shown that by using the self-similarity approach, it is possible to increase the gain value of the structure leading to the lower tensions and displacements on the strings. Furthermore, by changing the angle of the D-Bar, it is possible to increase or decrease the magnitude of the gains for the D-Bar. It is also shown that for displacement measurement, the angle α should be high whereas the force measurement case requires lower angle α for the higher magnitude of the gain.

Second, the stiffness analysis for the planar and 3D D-Bar systems are analyzed separately for their global stiffness under compressive loading condition. It is shown that as the angle α decreases, the stiffness increases for any complexity. This observation is valid for both the planar and 3D configurations. However, the stiffness behavior of the 3D D-bar system differs from the planar case for the increasing complexity. The increase in the number of the strings for 3D configuration dominates the stiffness formulation after a few self-similar steps and the stiffness tends to increase with the complexity in contrast to the planar configuration. Third, the mass of the planar D-Bar is derived subject to global stiffness requirements. However, checking the stiffness is not enough for this case. The yield condition for the strings should also be considered for the mass calculation of the strings.

Finally, a structure combining the D-Bar and the T-Bar is presented. The aim of such combination is to utilize both the minimal mass property of the T-Bar and the deployable property of the D-bar. The overall analysis showed that the $T_n D_1$ system can be employed as a deployable structure functioning as a sensor, actuator or both while satisfying a stiffness requirement and providing an optimum mass solution. Using these results, the paper shows how to design loaded platforms that can deploy to a specified shape while guaranteeing a specified stiffness and minimizing mass.

AUTHOR CONTRIBUTIONS

UB contributed to analytical calculations, generation of the examples and critical reading. RG contributed to generation of examples, critical reading and proofreading of the analytical expressions. RES contributed to development of the sensor/actuator concept and critical reading.

REFERENCES

- Calladine, C. R. (1978). Buckminster Fuller's tensegrity structures and Clerk Maxwell's rules for the construction of stiff frames. *Int. J. Solids Struct.* 14, 161–172. doi: 10.1016/0020-7683(78)90052-5
- Fuller, R., Applewhite, E., and Loeb, A. (1975). *Synergetics; Explorations in the Geometry of Thinking*. London: Macmillan.
- Goyal, R., Bryant, T., Majji, M., Skelton, R., and Longman, A. (2017). "Design and control of growth adaptable artificial gravity space habitats," in *AIAA SPACE and Astronautics Forum and Exposition* (Orlando, FL), 5141. doi: 10.2514/6.2017-5141
- Goyal, R., and Skelton, R. E. (2018). "Dynamics of class 1 tensegrity systems including cable mass," in *16th Biennial ASCE International Conference on Engineering, Science, Construction and Operations in Challenging Environments* (Cleveland, OH), 868–876. doi: 10.1061/9780784481899.082
- Hagiwara, Y., and Oda, M. (2010). "Transformation experiment of a tensegrity structure using wires as actuators," in *Mechatronics and Automation (ICMA), 2010 International Conference on* (Xi An), 985–990.
- Koizumi, Y., Shibata, M., and Hirai, S. (2012). "Rolling tensegrity driven by pneumatic soft actuators," in *Robotics and Automation (ICRA), 2012 IEEE International Conference on* 1988–1993. doi: 10.1109/ICRA.2012.6224834
- Motro, R. (2011). Structural morphology of tensegrity systems. *Meccanica* 46, 27–40. doi: 10.1007/s11012-010-9379-8
- Murakami, H., and Nishimura, Y. (2001). Static and dynamic characterization of regular truncated icosahedral and dodecahedral tensegrity modules. *Int. J. Solids Struct.* 38, 9359–9381. doi: 10.1016/S0020-7683(01)00030-0
- Nagase, K., and Skelton, R. E. (2014). Double-helix tensegrity structures. *AIAA J.* 53, 847–862.
- Pellegrino, S. (1986). *Mechanics of Kinematically Indeterminate Structures*. PhD thesis, University of Cambridge.
- Pugh, A. (1976). *An Introduction to Tensegrity*. Berkeley, CA: University of California Press.
- Rimoli, J. J. (2016). "On the impact tolerance of tensegrity-based planetary landers," in *57th AIAA/ASCE/AHS/ASC Structures, Structural Dynamics, and Materials Conference* (San Diego, CA), 1511.
- Skelton, R. (2005). "Dynamics and control of tensegrity systems," in *IUTAM Symposium on Vibration Control of Nonlinear Mechanisms and Structures* (Munich: Springer), 309–318.
- Skelton, R., and de Oliveira, M. (2009). *Tensegrity Systems*. Springer.
- Skelton, R., and Longman, A. (2014). "Growth capable tensegrity structures as an enabler of space colonization," in *AIAA Space 2014 Conference and Exposition* (San Diego, CA), 4370.
- Skelton, R. E., and de Oliveira, M. C. (2010). Optimal tensegrity structures in bending: the discrete michell truss. *J. Franklin Inst.* 347, 257–283. doi: 10.1016/j.jfranklin.2009.10.009
- Snelson, K. D. (1965). Continuous tension, discontinuous compression structures. US Patent 3,169,611.
- Sultan, C., and Skelton, R. (2004). A force and torque tensegrity sensor. *Sens. Actuat.* 112, 220–231. doi: 10.1016/j.sna.2004.01.039
- SunSpiral, V., Gorospe, G., Bruce, J., Iscen, A., Korbel, G., Milam, S., et al. (2013). Tensegrity based probes for planetary exploration: entry, descent and landing (EDL) and surface mobility analysis. *Int. J. Planet. Probes* 7.

Conflict of Interest Statement: The authors declare that the research was conducted in the absence of any commercial or financial relationships that could be construed as a potential conflict of interest.

Copyright © 2018 Boz, Goyal and Skelton. This is an open-access article distributed under the terms of the Creative Commons Attribution License (CC BY). The use, distribution or reproduction in other forums is permitted, provided the original author(s) and the copyright owner(s) are credited and that the original publication in this journal is cited, in accordance with accepted academic practice. No use, distribution or reproduction is permitted which does not comply with these terms.